



# Randomly iterated search and statistical competency as powerful inversion tools for deformation source modeling: Application to volcano interferometric synthetic aperture radar data

M. Shirzaei<sup>1</sup> and T. R. Walter<sup>1</sup>

Received 3 September 2008; revised 19 February 2009; accepted 5 May 2009; published 1 October 2009.

[1] Modern geodetic techniques provide valuable and near real-time observations of volcanic activity. Characterizing the source of deformation based on these observations has become of major importance in related monitoring efforts. We investigate two random search approaches, simulated annealing (SA) and genetic algorithm (GA), and utilize them in an iterated manner. The iterated approach helps to prevent GA in general and SA in particular from getting trapped in local minima, and it also increases redundancy for exploring the search space. We apply a statistical competency test for estimating the confidence interval of the inversion source parameters, considering their internal interaction through the model, the effect of the model deficiency, and the observational error. Here, we present and test this new randomly iterated search and statistical competency (RISC) optimization method together with GA and SA for the modeling of data associated with volcanic deformations. Following synthetic and sensitivity tests, we apply the improved inversion techniques to two episodes of activity in the Campi Flegrei volcanic region in Italy, observed by the interferometric synthetic aperture radar technique. Inversion of these data allows derivation of deformation source parameters and their associated quality so that we can compare the two inversion methods. The RISC approach was found to be an efficient method in terms of computation time and search results and may be applied to other optimization problems in volcanic and tectonic environments.

**Citation:** Shirzaei, M., and T. R. Walter (2009), Randomly iterated search and statistical competency as powerful inversion tools for deformation source modeling: Application to volcano interferometric synthetic aperture radar data, *J. Geophys. Res.*, *114*, B10401, doi:10.1029/2008JB006071.

## 1. Introduction

[2] High-resolution mapping of spatiotemporal deformation fields can provide important information about earthquake and volcanic source geometries and associated physical processes. Utilizing numerical and analytical modeling techniques, detected deformation signals can be theoretically reproduced. This would enable, for instance, the determination of the specific characteristics of a magma chamber. The inferred characteristics of the magma chamber (or “source”) can include diverse geometric parameters such as location and volume or pressure change. These physical variables are especially important for hazard assessment, including volcano monitoring or fast response teams.

[3] Since the relation between surface deformation and magmatic sources of Japanese volcanoes has been investigated via an analytical formulation of an inflating point source in an elastic half-space [Mogi, 1958], many other

developments in the field of analytical models and their applications have been achieved to constrain magmatic source parameters specifically based on surface deformation data. Okada [1985] presented a closed formulation to explain parameters of a rectangular dislocation source causing surface deformation in an elastic half-space. This model is applicable to volcanic and earthquake simulation, treating the source as a finite rectangular fault that is either subject to opening, or subject to strike and dip slip motions. Shortly afterward, Davis [1986] presented an analytical expression of an ellipsoidal inflating cavity buried in an elastic half-space that causes deformation at the surface and enables exploration of the surrounding stress field. This research was ground for other developments, such as an analytical expression of a finite sphere in half-space [McTigue and Segall, 1988] and pressurized dipping ellipsoidal source [Yang *et al.*, 1988]. Despite their simplicity, these models have successfully explained observed deformation fields resulting from volcanic and tectonic activities over the past 60 years [Dzurisin, 2006], which together with independent geophysical and geological evidence has demonstrated the validity of these kinds of analytical expressions to define the geometrical and mechanical parameters of the source of deformation.

<sup>1</sup>Section 2.1, Department of Physics of the Earth, Deutsches GeoForschungsZentrum, Potsdam, Germany.

**Table 1.** Summary of Selected Optimization Methods Used in Different Branches of the Geosciences

Method	Main Idea	Application	Advantage	Disadvantage
Least squares	Gradient based	<i>Lundgren et al.</i> [2001], <i>Jónsson et al.</i> [2002], <i>Battaglia et al.</i> [2003, 2006], and <i>Lanari et al.</i> [2004]	Very fast for convex search space	May get trapped in local minima.
Monte Carlo	Randomly samples the parameters space	<i>Keilis-Borok and Yanovskaja</i> [1967]	Gradient free	Slow. May miss the global solution.
Neighborhood algorithm <sup>a</sup>	Generate new samples with density function related to previous step samples	<i>Sambridge</i> [1998, 1999a, 1999b] and <i>Amoruso et al.</i> [2007]	Gradient free	Slows down very significantly when the number of parameters increases.
Simulated annealing <sup>a</sup>	Motivated by analogy between annealing in solids and optimization problems	<i>Cervelli et al.</i> [2001b], <i>Chevrot</i> [2002], <i>Jónsson et al.</i> [2002], and <i>Amelung et al.</i> [2007]	Gradient free, fast	Slows down when the number of parameters increases. Success depends on the cooling schedule. May find a solution in the vicinity of the global solution.
Genetic algorithm <sup>a</sup>	Motivated by analogy between biological evolution and optimization problems	<i>Currenti et al.</i> [2005], <i>Gottsmann et al.</i> [2006], and <i>Carbone et al.</i> [2008]	Gradient free, fast	Slows down when the number of parameters increases. May find a solution in the vicinity of the global solution.

<sup>a</sup>These methods are basically inspired by Monte Carlo search approach and fall into the same class.

[4] The procedure for obtaining the parameters of an analytical model from an observed displacement field is an inverse problem. From a mathematical point of view, there are many different techniques for solving an inverse problem and, therefore, for investigating magma chamber processes (see Table 1). A sophisticated inversion (optimization) technique requires a balance of robustness and efficiency. Geophysical solutions that have been presented in the literature often provide details about the location and/or strength of a deformation source without knowing the sensitivity of the data and/or the model, which is directly related to the quality of the result. In order to evaluate the robustness of an inversion, the sensitivity of source parameters to the observations must be evaluated first. Moreover, because space geodetic data sets are spatially and temporally increasingly large, the handling of this quantity of data together with their full variance-covariance matrix reflecting observation quality and relative weight has become a major difficulty in optimization problems. Several algorithms have been proposed to downsample such large data sets, including either sophisticated approaches such as Quadtree sampling [*Jónsson et al.*, 2002] or simple methods such as uniform sampling. Although these methods principally downsample the observation field, some important data may be lost. Therefore, as an alternative, improved and faster inversion algorithms may allow use of a more complete or even full data set.

[5] In this paper, we investigate the robustness and efficiency of optimization techniques with a focus on two sophisticated commonly used methods: the simulated annealing (SA) and genetic algorithm (GA). In comparison to other optimization techniques, SA and GA have been shown to be excellent methods for finding global solutions in complex search spaces [*Sambridge and Mosegaard*, 2002], which encourages researchers in various geophysical disciplines to use these methods for optimization (Table 1). We evaluate the advantages and disadvantages of these methods and find that GA, in general, and SA, in particular, may get trapped in local minima. Therefore, we suggest

including a new iterative approach and statistical competency test to elude local traps and to estimate the reliability of the solution, thus improving the quality of the result.

[6] The paper is organized as follows. First, in synthetic tests, we consider analytical models of different sources as an effective component governing the interaction of observation and inversion parameters. The investigated sensitivity allows us to estimate how a model may affect the precision and accuracy of inversion results. Second, we explain SA and GA optimization methods and show which parameters are important for the algorithm to successfully find a global solution. Third, we apply a randomly iterated search approach in order to avoid local minima and reduce the effect of the “cooling schedule.” We suggest that a statistical competency (SC) approach, considering both observation uncertainty and model deficiency, may allow estimation of the source parameters and their quality. Finally, we demonstrate the robustness and efficiency of our improved algorithms via synthetic tests and apply the two different methods to periods of uplift (2000–2001) and subsidence (2001–2002) at the Campi Flegrei caldera volcano, Italy.

## 2. From Data to Dislocation Model

[7] In the last two decades, the GPS and InSAR technique have provided nearly continuous observation of deformation fields in time (case for GPS) and in space (case for InSAR). With precision better than 1 cm, these techniques have increased the ability to develop a reasonable interpretation of geodetic data and also to analyze physical processes. One of the most common applications of these observations is to numerically or analytically simulate the source of the deformation. Three widely used analytical models for simulating the source of deformation events are the point source [*Mogi*, 1958], including four parameters (two horizontal locations, depth, and strength); the ellipsoidal source [*Yang et al.*, 1988], including eight parameters (two horizontal locations, depth, semi major and semi minor axes, plunge and strike angle of major axis, and pressure

change); and the rectangular source [Okada, 1985], including ten parameters (two horizontal locations, depth, length, width, dip, strike, and three dislocation components). The first two source types are commonly used for volcano and reservoir modeling, while the last is applicable to both volcanic and earthquake events. All of these models are usually implemented in an isotropic, linear, homogeneous, elastic half-space. Despite their simplicity, in many examples these models can explain surface deformations very well and are used as standards in modern geodesy (Table 1). However, their sensitivity has been only partly investigated [Dawson and Tregoning, 2007] and for volcanic sources not characterized in detail. In the next sections, we will summarize the mathematical relations to obtain model parameters based on surface observation and perform a sensitivity analysis to test the effect of the three source parameters on the surface deformation field.

### 2.1. Dislocation Problem and Optimization

[8] The stochastic model relating surface deformation data to dislocation source parameters is:

$$L + v = F(S) \quad (1)$$

where  $L$  is deformation observation,  $F$  is a function that provides a mathematical relation between deformation data and source parameters  $S$ , and  $v$  is the observation residual. As  $m$  is the number of observations and  $n$  is the number of source parameters, usually  $m > n$ . In this case, the number of unknowns is  $m + n$ , which means that equation (1) has many solutions. We are interested in a solution that minimizes a function of  $v$ . On the basis of this approach, to estimate the source parameters, we solve an optimization problem:

$$C(v, P) \rightarrow \min \quad (2)$$

where  $P = \sigma_0^2 C_l^{-1}$  is a weight matrix of the observations,  $C_l$  is variance-covariance matrix of the observations,  $\sigma_0^2$  is the primary variance factor, and  $C$  is a function of  $P$  and  $v$  constraining the solution space [Vanicek and Krakiwesky, 1982]. The most frequently used cost function in optimization problems is the weighted second norm of the residuals, given by

$$C(v, P) = v^T P v \quad (3)$$

The advantages of this cost function are an unbiased estimation of the source parameters [Bjerhammar, 1973] and a chi-square probability density function of  $v^T C_l^{-1} v$ , which may be used for evaluating the result [Vanicek and Krakiwesky, 1982]. Because of the latter advantage, a confidence interval  $\chi_{n-m, \alpha/2}^2 < v^T C_l^{-1} v < \chi_{n-m, 1-\alpha/2}^2$  in a confidence level of  $(1 - \alpha) \%$  can be defined. This test can be rejected from the right side or left side. Rejection from the right side may mean a defect in the model or observation. Left side rejection means the residuals are too small or the model is too good. This could be the case in modeling the source of crustal deformation, where the easiest and unrealistic way to obtain a small residual is by adding more and more analytical sources (e.g., point sources) without any constraints or auxiliary information. In this case, despite

having an excellent fit to the observations, the analytical model may be completely wrong. For example, a point-wise observation of ground displacement (e.g., by GPS) can be perfectly fitted by defining dislocation sources of the deformation field at each of the observation points, even though the physical sense of such a model is questionable. As a result, during the optimization one should be aware of possible model defects as well as observation defects, keeping in mind that the model with the best fit is not always the most realistic solution. In the following, we assess the quality of the results and the models.

### 2.2. Sensitivity Analysis of Three Different Analytical Models

[9] The mutual effect of dislocation parameters and deformation field observations is studied by a model sensitivity analysis. A sensitivity analysis is herein referred to as a study of the two-way relationship between observations and parameter variations that are related via an analytical model. Using a Taylor series in matrix format, equation (1) can be expressed as

$$\widehat{L} = GS \quad (4)$$

where  $\widehat{L} = L + v$  and  $G = \partial F / \partial s$  is a coefficient matrix reflecting the model effect [Vanicek and Krakiwesky, 1982]. The relationship between a change in the parameters  $\Delta S$  and a change in the observation  $\Delta L$  is obtained from  $\Delta L = G \Delta S$ . Using the definition of the generalized inverse and norm for matrices,  $\|\Delta S\| \leq \|G^{-}\| \|\Delta L\|$ , where  $\|G^{-}\|$  is the inverse of  $G$ . Dividing both sides of the latest inequality by  $\|\widehat{L}\|$  yields a relation between parameters and observation relative error:

$$\frac{\|\Delta S\|}{\|S\|} \leq \|G\| \|G^{-}\| \frac{\|\Delta L\|}{\|\widehat{L}\|} \quad (5)$$

where  $\|G\| \|G^{-}\|$  is the condition number of the coefficient matrix (considering the Euclidean norm, the condition number is equal to the ratio of largest to smallest singular value). Equation (5) provides an upper bound for the relative error of the parameters or a lower bound for the relative error of the observations.

[10] In other words, when the condition number is small,  $\|\Delta S\| / \|S\|$  would be small if  $\|\Delta L\| / \|\widehat{L}\|$  is small, and, when the condition number is large,  $\|\Delta S\| / \|S\|$  can be large even if  $\|\Delta L\| / \|\widehat{L}\|$  is small. Equation (5) shows that observation and parameter error influence each other and also that this mathematical relationship may play an important role in the propagation and estimation of the error. Knowing these interactions between the model, observations, and parameters, we examine the three aforementioned types of analytical dislocation sources having 4, 8, and 10 parameters to be resolved, respectively. For this purpose, we assumed a reference state for the source parameters (Table 2) and studied the effect of parameter fluctuations on observations through forward modeling. In order to simulate a realistic scenario and to compare the results to the real data sets in section 5, observations are displayed along the line of sight (LOS) of the ERS radar satellite (descending orbit, incidence angle  $23^\circ$ , azimuth  $190^\circ$ ) shown along an east-

### Sensitivity test for Mogi source

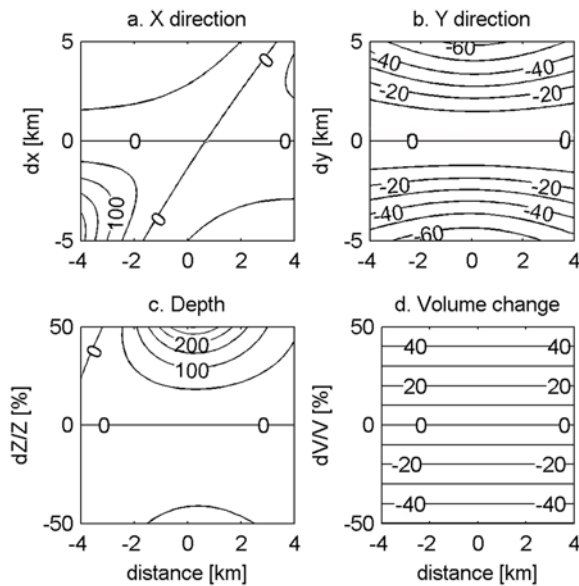


**Figure 1.** Sensitivity test of the Mogi-type dislocation source parameters to observed deformation perturbation in the LOS direction of ERS radar images in descending mode. We considered a profile in the west-east direction and calculate the LOS observation due to relative changes of the selected source parameters. Observation relative error is presented versus the relative error of the parameters at different distances (ordinate). In Figures 1a–1d, the  $x$  axis is the horizontal distance from the source, and only one parameter changed, while the rest are fixed at the reference value (Table 2). The contour line shows the relative change in LOS observation in percent; a positive value for the contour line indicates overestimating the reference LOS, while negative value indicates underestimating those. The mutual effect of LOS displacement change and (a)  $X$  coordinate perturbation, (b)  $Y$  coordinate perturbation, (c) source depth relative perturbation (overestimation/underestimation), and (d) source volume relative change is shown.

west profile in Figures 1–3. By choosing an east-west profile we investigated the highest level of sensitivity that results from the satellite geometry. The reader can expect less sensitivity for direction profiles other than the east-west. In Figures 1–3, only one parameter is altered, and the rest are fixed at the reference value. The relative error of observation (reference value minus calculated value divided by reference value) is presented as a function of the parameter relative error and distance; i.e., a high percentage of relative change ( $>50\%$ ) means high sensitivity of the parameters to observation fluctuation and vice versa.

[11] For a Mogi-type point source (Figure 1), we found a direct relation between observation and parameter changes. A large change of location ( $X$ ,  $Y$ ,  $Z$ ) and a large volume change ( $dV$ ) caused large changes in the observation and vice versa. This effect was symmetric for  $Y$ ,  $Z$ , and  $dV$ ; however, the effect for  $X$  appeared distorted because of the observation geometry. We found an exception in the result for parameter  $X$  (Figure 1a), where large alterations in the  $X$  coordinate ( $\sim -5$  km) did not influence the LOS obser-

variations at distances of about 1.8 km from the origin. This poor interaction between the parameters and the observations was the result of a defect in the analytical model (poor condition number). In another exceptional behavior, observed in Figure 1c, where the interaction between parameter  $Z$  and the observations are investigated, a positive depth alteration (i.e., shallower source) significantly influenced the observations located around the origin. This behavior is probably because of the invalidity of modeling shallow

### Sensitivity test for Yang source

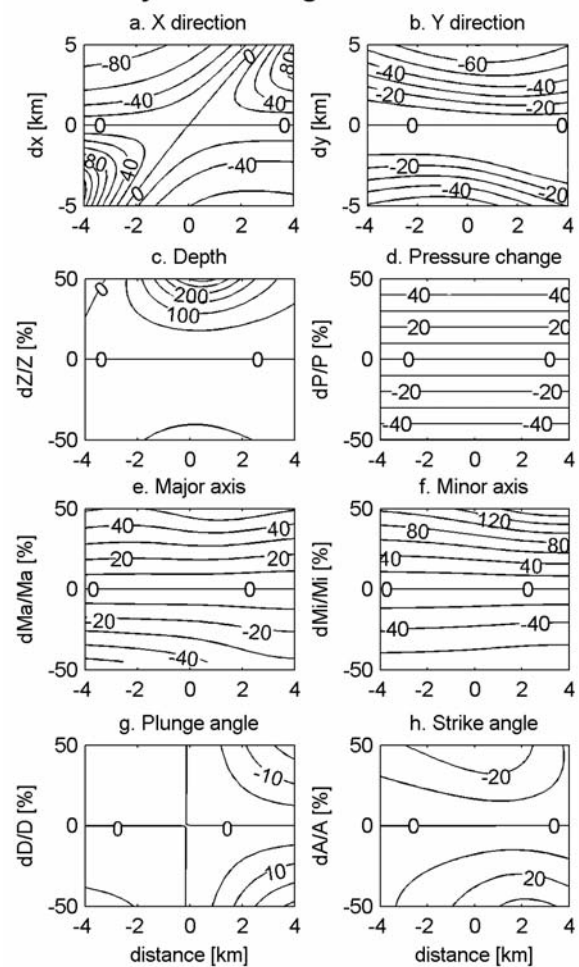


**Figure 2.** Sensitivity test of the Yang-type source parameters and observed deformation perturbation in the LOS direction of ERS radar images in descending mode. Profile in the west-east direction shows LOS observation for the parameters given in Table 2. In Figures 2a–2h, the  $x$  axis is horizontal distance from the source, and all parameters but one are fixed at the reference value; that is, the contour line shows relative change with respect to the reference situations (Table 2). Positive value for the contour line indicates overestimating the reference LOS, while negative value indicates underestimating those. The interaction of the LOS displacement relative change and (a)  $X$  coordinate perturbation, (b)  $Y$  coordinate variations, (c) source depth relative undulation (overestimation/underestimation), (d) source pressure relative change, (e and f) source semimajor/minor axis relative variations, and (g and h) source plunge/strike angle relative perturbation is shown.

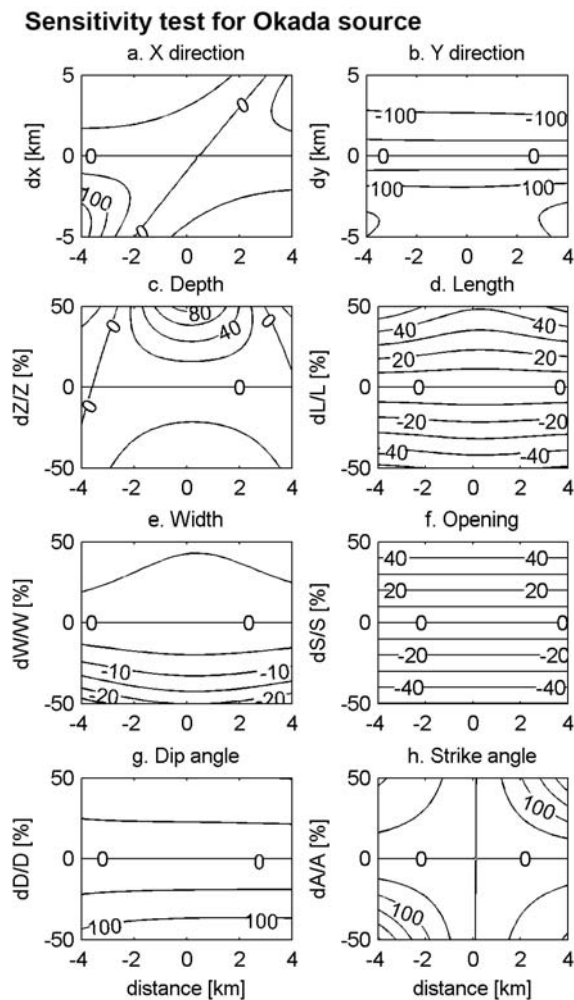


**Figure 3.** Sensitivity test of the Okada-type source parameters and observed deformation. Profile in the west-east direction shows the LOS observation for the parameters given in Table 2. In Figures 3a–3c, the  $x$  axis is the horizontal distance from the source center, and all parameters but one are fixed at the reference value; that is, the contour line shows relative change with respect to the reference situation (Table 2). Positive value for contour line indicates overestimating the reference LOS while negative value indicates underestimating those. The interaction of the LOS displacement change and (a) X coordinate perturbation, (b) Y coordinate perturbation, (c) source depth relative undulation (overestimation/underestimation), (d) source length relative perturbation, (e) source width relative perturbation, (f) source opening relative perturbation, and (g and h) source dip/strike angle relative perturbation is shown.

deformation sources as point sources, which can be categorized in terms of model deficiency. The sensitivity test of a Mogi source model thus suggests that, for reliable estimation of the parameter locations and volume changes, good coverage of the observation field is required in addition to precise and accurate observations.

[12] For an ellipsoidal Yang-type source (Figure 2), we show the sensitivity test for the eight source parameters. We found that most parameters show a direct and almost symmetric relation to observation error. Positive errors in

depth led to the same effect as positive errors in the depth of Mogi models which may imply that this model is valid for deep sources as discussed by *Yang et al.* [1988]. In the case of the plunge and strike angle (Figures 2g and 2h), a change of parameters by about 50% had very little effect on the near-field observations. The plunge and strike angle can only be constrained by a few percent in the far field. The sensitivity test of the Yang-type source thus suggests that a very broad observation field is required to reliably estimate the ellipsoidal source parameters, including data from the near field (to constrain location and strength) and the far field (to constrain plunge and strike). Note that the definition of the “near-field” region is case-dependent. For example, this region will be broader than shown in this example for a deeper source.

[13] The sensitivity tests for a rectangular Okada-type source are shown in Figure 3. Considering only opening mode dislocations left us with eight parameters to be tested for sensitivity. The situation was generally similar to the above described Yang-type source, showing a symmetric and direct relationship between the observation and parameter error. The parameter width  $W$  (Figure 3e) shows a small sensitivity to LOS observation. For the chosen simulations, the strike angle had no effect on the near-field observation. The sensitivity test for the Okada plane thus shows that good sensitivity is obtained for the coordinate, length, opening, and dip angle parameters. Moreover, it suggests that both good coverage and observation accuracy are necessary for a reliable estimation the source parameters. The parameters width and strike cannot be resolved uniquely unless additional data sets (such as far-field geodetic or seismic data) are included.

[14] Considering the three sensitivity tests, we can summarize that the source parameters are affected differently by the precision and spatial distribution of the observations, which are important in qualifying the result. In the sensitivity test, the influence of the observation precision could be drawn by considering equation (5), where observation precision ( $\Delta L$ ) is related to parameters error ( $\Delta S$ ). By having high-precision observation (small  $\Delta L$ ) we are able to constrain slight changes in parameters (small  $\Delta S$ ), even though the problem is governed by a poor condition number. For reliable and precise source inversion, therefore, good coverage including both near- and far-field data is necessary in order to obtain adequate sensitivity. On the other hand, increasing the number of data, e.g., by considering two satellite viewing geometries (e.g., ascending and descending), may only lead to somewhat improved results. And it may leave some of the model parameters nonunique (see the auxiliary material).<sup>1</sup> With this knowledge of the limitations of simple analytical models, we are able to test the influence of different inversion algorithms on source parameter estimation in section 3.

### 3. A Comparison of Sophisticated Optimization Methods

[15] In the case of early warning and semi-real-time hazard assessment of crustal deformation activities, a fast

<sup>1</sup>Auxiliary materials are available in the HTML. doi:10.1029/2008JB006071.

**Table 2.** Parameters of Three Different Deformation Source Types Used in Synthetic Tests<sup>a</sup>

	X (km)	Y (km)	Depth (km)	Strength			Length/Maj. Ax (km)	Width/Min. Ax (km)	Dip/Plunge (deg)	Strike (deg)
				Vol. Ch (km <sup>3</sup> )	Pr. Ch (GPa)	Op (m)				
Mogi (point)	0	0	5	0.01			-	-	-	-
Yang (ellipsoid)	0	0	5		0.01		2	1	45	45
Okada (rectangular)	0	0	5			2	3	2	45	135

<sup>a</sup>Source types are point, ellipsoidal, and rectangular. After *Mogi* [1958], *Yang et al.* [1998], and *Okada* [1985]. X, Y, horizontal coordinates; Depth, depth to source center (for Mogi and Yang sources) or depth to upper edge (for Okada source), Vol. Ch, volume change for Mogi source; Pr. Ch, pressure change for Yang source; Op, opening for Okada source; Length, length of Okada plane; Maj. Ax, major axis of Yang source; Width, width of Okada plane; Min. Ax, minimum axis of Yang source; Dip, dip angle for Okada plane or Plunge angle for Yang source; Strike, strike angle of Okada plane or strike angle of Yang source major axis.

and reliable evaluation of deformation sources is very important. Considering this demand, an inversion tool that is gradient free (i.e., free from initial values), reliable, efficient, and flexible enough to include other complementary information is required. For nearly 30 years the simulated annealing (SA) and genetic algorithm (GA) have been used for data inversion purposes (Table 1). This is because SA and GA are gradient free, which is important for fast source assessment (case for early warning systems), and because of their success in solving a large variety of optimization problems in different branches of the geosciences [*Sambridge and Mosegaard*, 2002]. Apart from those optimization methods addressed in Table 1, many other novel optimization methods have recently emerged. However, among them, the so-called covariance matrix adoption evolutionary strategy (CMA-ES), which is a stochastic method for the optimization of nonlinear and nonconvex functions is showing merits for solving optimization equations with few (<100) number of parameters [*Igel et al.*, 2007]. However, the choice of initial parameters plays a significant role in the success of this method. Moreover, the diversity of the search operator to explore the search space critically depends on the settings of the normal distribution function, which is often problem-dependent.

[16] In sections 3.1–3.3, we briefly explain the concepts and disadvantages of these two most commonly used optimization methods, GA and SA. We then propose an improved algorithm that allows joint estimation of the uncertainty of the parameters. The proposed algorithm may be applied to other optimization methods as well.

### 3.1. Simulated Annealing

[17] The simulated annealing (SA) algorithm is motivated by an analogy to annealing in solids [*Metropolis et al.*, 1953], which has been applied to optimization problems for the last 25 years [*Kirkpatrick et al.*, 1983]. Generally, SA starts with a random initial value of parameters, with an associated score based on the cost function, and a cooling schedule that includes the initial temperature, the reduction rate of temperature, the number of generated events at each temperature, and a final temperature to stop the algorithm [*Kirkpatrick et al.*, 1983]. A commonly used cost function is presented in equation (3). The orders of major steps in SA are introduced by different temperatures. At each temperature, small random changes are added to the parameters, and the resulting change in cost ( $\Delta c$ ) is computed. If  $\Delta c \leq 0$ , the change is accepted; otherwise, the change is treated probabilistically. The probability density function (PDF) of

$\Delta c$  at the current temperature  $T$ , with the Boltzmann coefficient  $K_B$ , is  $\text{PDF}(\Delta c) = e^{-(\Delta c/K_B)T}$  [*Kirkpatrick et al.*, 1983]. If  $\text{PDF}(\Delta c)$  is greater than a random number uniformly selected in the interval (0,1), then the change is accepted.

[18] The success of SA at finding a global solution critically depends on the cooling schedule [*Rothman*, 1985; *Basu and Frazer*, 1990; *Cervelli et al.*, 2001a]. Although a slow cooling schedule at the expense of computation time might be useful, the difficulty is that the cooling schedule is substantially problem-dependent, and it seems impracticable to develop a global remedy for all problems. To overcome those limitations, SA is sometimes combined with other optimization techniques [*Cervelli et al.*, 2001a]. Another shortcoming is that an estimation of the parameters' quality is missing.

### 3.2. Genetic Algorithm

[19] The genetic algorithm (GA) was introduced by *Holland* [1975] and further improved by many subsequent researchers [*Davis*, 1987; *Goldberg*, 1989; *Rawlins*, 1991; *Whitley*, 1994] who have provided comprehensive summaries on the theory and applications.

[20] In the basic form of GA [*Holland*, 1975], a key aspect is the binary encoding of the parameters. The search begins by defining a cost function and initializing the GA parameters, and it ends when a stopping criterion, such as the defined number of iterations, is reached. GA always deals with a set of solutions without any special emphasis on a particular solution. So, if the initial population consists of  $m$ -independent solutions, each solution includes  $n$  variables, and each variable can be presented by  $q$  bits, then the initial population is constructed randomly by  $n \times (m \times q)$  zeroes/ones. To evaluate the cost function, we need the decimal values of the variables obtained by [*Haupt and Haupt*, 2004]

$$p_q = \sum_{i=1}^q g(i)2^{-i} + 2^{-(i+1)} \quad (6)$$

$$p = p_q(u_b - l_b) + l_b \quad (7)$$

where  $l_b$  and  $u_b$  are lower and upper limits and  $p$  is the corresponding decimal value of the binary variable  $g$ . Because we have prior knowledge about the variables in many problems, equations (6) and (7) allow entering this kind of auxiliary information into an inversion procedure by setting the limits for the variables during decoding.

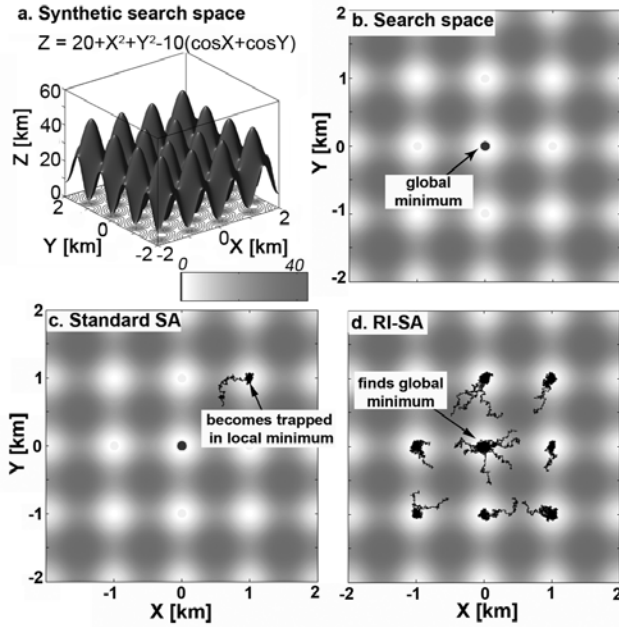


**Figure 4.** Synthetic search space to test local and global minima trapping and advancements of the RI approach. Standard SA and randomly iterated (RI) SA are both initialized with the same cooling schedule. (a) A 3-D mesh of the synthetic search surface which has many local minima but only one global minimum of 0 at (0, 0), (b) plan view of the search space, with the global minimum depicted by solid circle; (c) the trace of a standard SA test is converging to a local minimum at (1, 1) and fails to find the global minimum, and (d) the trace of RI-SA is initialized iteratively at random starting points and finally finds the global minimum.

[21] During the algorithm progress, the initial population is subject to several random changes but systematically approaches the best solution among many investigated solutions. Selection, pairing, mating, and mutation are major GA operators that allow modification of the population to explore solution space, and they are thoroughly explained in the literature [Holland, 1975, 1992; Michalewicz, 1994].

[22] Despite remarkable successes in solving very complex optimization problems, GA does not provide any information about the quality of the results. Some researchers have implemented approaches to estimate a symmetric PDF of the model variables after optimization [Zhou *et al.*, 1995]. However, the assumption of symmetry is true only when the relation between the observation and model parameters is linear. Carbone *et al.* [2008] used the approach presented by Deb *et al.* [2000] to estimate a confidence region for parameters free of any primary PDF assumptions. Quality estimation in this approach relies on the inversion residuals. The success of this approach depends on the freedom of the search operator to explore the vicinity of the optimum solution. Therefore, mutation rate and population size may play a significant role in the reliability of the result. Additionally, these approaches do not consider the effect of a model on the optimization result. Therefore, careful assessment of the result quality is still missing.

[23] In brief, the main shortcomings of the SA and GA are (1) getting trapped in local minima and (2) lack of estimation of the quality of the parameters. Therefore, in the following, we introduce and test the hybrid randomly iterated search (RI) and statistical competency (SC) approach.

### 3.3. Randomly Iterated Search

[24] In order to diminish the importance of the cooling schedule (case for SA) and to increase the freedom of the search algorithm to explore the solution space (case for SA and GA), which is a necessity in statistical approaches for estimating the confidence interval, we present and apply a randomly iterated search. The idea is to repeat the optimization with different initial random values in order to begin the search from a starting point close to the global solution. Here, we explain a combination of a randomly iterated search (RI) with SA. Via a synthetic test, we show the improvement of RI-SA compared to the standard SA. We then compare our random approach to the standard SA presented by Kirkpatrick *et al.* [1983]. Both algorithms are initialized with the same cooling schedule. As shown in Figure 4, the cost function is a mathematical function that includes many local minima, but only one global minimum of 0 at coordinate (0, 0). Having the coordinates (0.6, 0.6) as a starting point, Figure 4c shows the trace of the standard SA searched for a global minimum but ultimately missed it and converges to a local minimum at coordinate (1, 1). In contrast, the RI-SA (Figure 4d) was initiated at various random starting points (here 20, Figure 4d) with the same cooling schedule and finally converged to the global minimum even in this difficult synthetic test. Thus, it is clear that RI-SA is able to find a global solution, while the other solutions in its vicinity can be used for qualifying the solution as detailed below.

### 3.4. Statistical Competency

[25] To test the statistical competency (SC) of the result of the SA, the optimization algorithm may be repeated  $p$  times starting from  $p$  initial points  $\{I_1, I_2, \dots, I_p\}$  selected randomly between a lower and upper limit. These limits can be specified on the basis of auxiliary information provided by other disciplines such as geologic measurements or earthquake hypocenters. Note that theoretically, the auxiliary information only facilitates the speed of convergence and will not affect the final result. In the RI-SA, we save all acceptable solutions with their associated cost. After sorting acceptable solutions based on increasingly cost value in each repetition, we select the  $q_i (i : 1 \dots p)$  best solutions to yield  $p$  subsets  $\{S_1\}, \{S_2\}, \dots, \{S_p\}$  with an average cost of  $\mu_{s_i} (i : 1 \dots p)$  as representative. The threshold can be specified either as a certain portion of the observations, based on the chosen cost function, or simply as a random number. The solution with the minimum cost among the subsets approaches the global solution  $\mu$ . Each representative has a standard deviation  $\sigma_{s_i}$  and  $E\{\mu_{s_i}\} = \mu$  ( $E$  is expectation operator). In order to construct a confidence interval for  $\mu$  when the variance is unknown, we may utilize the following statistic [Vanicek and Krakiwesky, 1982]:

$$\frac{\mu_{s_i} - \mu}{\sigma_{s_i} / \sqrt{q_i}} \quad (8)$$

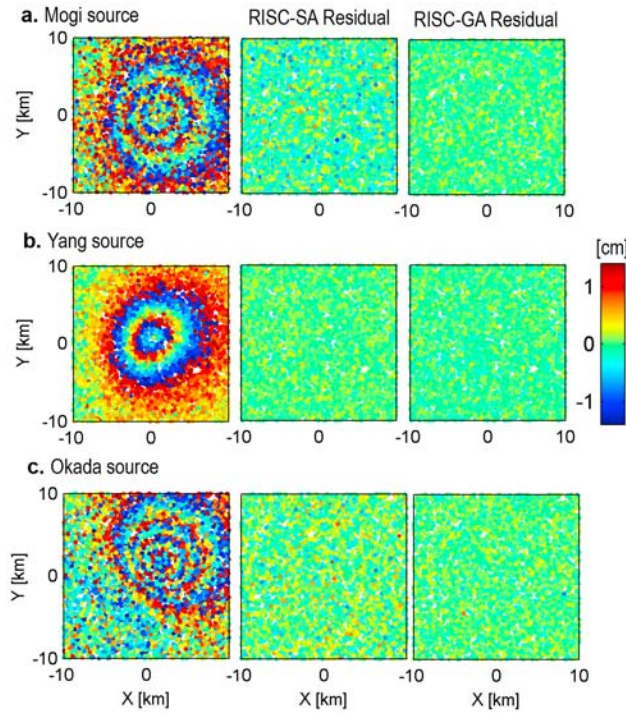


**Figure 5.** Synthetic test to show the reliability and efficiency of the randomly iterative search and statistical competency (RISC) SA and GA and to compare their result. Source parameters are given in Table 2 for three different source types. The observations are in the LOS direction of the descending ERS radar images, and a noise component was added with normal distribution (0, 0.6). (left) The models, (middle) the residuals of the RISC-SA, and (right) the residuals of the RISC-GA. (a) Mogi-type source deformation field, (b) Yang-type source deformation field, and (c) Okada-type source deformation field.

Equation (8) has a t distribution function [Vanicek and Krakiwesky, 1982], and, by specifying a significance level  $\alpha$  (or confidence level,  $1 - \alpha$ ), the confidence interval for  $\mu$  can be expressed as

$$\mu_{s_i} - \frac{t_{\alpha/2, (n-m)}}{\sigma_{s_i} / \sqrt{q_i}} \leq \mu \leq \mu_{s_i} + \frac{t_{\alpha/2, (n-m)}}{\sigma_{s_i} / \sqrt{q_i}} \quad (9)$$

If this test fails, the solution is rejected. If this test is accepted, the solution in the vicinity of the best solution is used to construct the confidence interval. After testing all solutions in equation (9), the accepted solutions contain a confidence interval for unknowns and thus allow evaluation of the result. The same successful approach can also be applied to other algorithms, as detailed in the following for GA.

[26] To achieve a statistical competency (SC) test of the GA result, we consider a large population size with random members for optimization in  $p$  iterations (randomly iterated search (RIS)) and select  $q_i (i : 1 \dots p)$  to be the best solutions in each generation. After satisfying the stopping criteria, there are  $p$  sets:  $\{S_1\}, \{S_2\}, \dots, \{S_p\}$ . Each set has  $q_i$  chromosomes with an average cost of  $\mu_{s_i} = (i : 1 \dots p)$  as a representative. The solution with minimum cost among all the subsets is termed  $\mu$ . Then, each  $\mu_{s_i}$  has a standard deviation  $\sigma_{s_i}$  and  $E\{\mu_{s_i}\} = \mu$ . The rest of the algorithm used

to build up a confidence interval is comparable to equations (8) and (9). One should note that the statistics is built upon the residuals after evaluating in the cost function (equation (3)), and the required independency for the t distribution is preserved by a random error that tainted the observations. However, to assure this independency and preserve diversity of the solutions in the vicinity of the global solution the mutation rate should be large enough ( $>0.5$ ) and repeated generations are eliminated from each sets.

[27] In summary, for both RISC-SA and RISC-GA, we simultaneously considered the effects of observation variance via a weight matrix and observation blunder, together with model deficiencies through defined statistics. In the next section, we shall show that the solution is precise (with small dispersion around the average) and accurate (the average is close to the true value).

#### 4. Application to Synthetic InSAR Data

[28] The reliability and efficiency of the described optimization techniques are first investigated in synthetic tests (section 4) and then applied to real observations (section 5). To organize the simulated data sets, we consider the same source types as in the sensitivity tests of section 2 (point, ellipsoidal, and rectangular sources). In reality, the observations are tainted by different random and systematic errors, but in the current test, we assume that the observations are free of systematic errors. To consider the effect of random noise, we add a normally distributed component with a variance of 0.5 cm to the observations. This variance is comparable to the real variance of modern radar interferometric methods [Berardino *et al.*, 2002]. Figure 5 shows a synthetic surface deformation at 5000 randomly distributed points calculated for a point source (Mogi, Figure 5a), an ellipsoidal source (Yang, Figure 5b), and a rectangular source (Okada, Figure 5c). We invert these three data sets using the inversion algorithms detailed in section 3 and discuss the results. The MATLAB script utilized for this test can be found in the auxiliary material.

[29] For the Mogi model (Figure 5a), we run the optimization algorithm in a limited search space to explore the solution area. This information can be obtained either from other disciplines like geological and seismological data or from some trade-off free equations that give a rough estimate of the parameters directly from the observed displacement field. Here, we estimate the relation between volume change occurring at the source in elastic half-space (Poisson ratio of 0.25), and observed LOS displacement with an incidence angle of  $\theta = 23^\circ$  for a Mogi source according to (see the auxiliary material for mathematical proof):

$$\Delta v = 0.72 \iint_{R^2} \text{LOS} \, dx dy \quad (10)$$

Equation (10) is independent of the source depth and provides an estimate of the volume change based on LOS observations. In a real case, we would have had access to only a small part of the displacement field; hence, this estimate might be considered as a lower limit for the volume change in the optimization process.

[30] On the basis of equation (10), the approximate volume change is  $6 \times 10^{-3} \text{ km}^3$ . The RISC-SA parameters

**Table 3.** Inversion Results of the Synthetic Deformation Field<sup>a</sup>

Parameter	Simulated Algorithm		Genetic Annealing	
	Inversion Result	Confidence Interval (95%)	Inversion Result	Confidence Interval (95%)
<i>Mogi</i>				
X (km)	-0.02	(-0.14, 0.16)	0.33	(-0.72, 0.12)
Y (km)	-0.04	(-0.26, 0.29)	-0.02	(-0.39, 0.45)
Depth (km)	5.05	(-0.32, 0.34)	4.93	(-0.32, 0.64)
Volume change (km <sup>3</sup> )	0.0101	(-0.0009, 0.0009)	0.0099	(-0.0016, 0.0023)
<i>Yang</i>				
X (km)	0.05	(-0.44, 0.05)	0.14	(-0.57, 0.34)
Y (km)	-0.08	(-0.31, 0.43)	0.18	(-0.58, 0.4)
Depth(km)	4.84	(-0.33, 0.41)	4.95	(-0.2, 0.53)
Pressure change (GPa)	0.0138	(-0.0065, 0.0007)	0.0078	(0, 0.0102)
Major axis (km)	1.90	(-0.37, 0.45)	2.18	(-0.41, 0.01)
Minor axis (km)	0.88	(-0.005, 0.23)	1.06	(-0.4, 0)
Plunge (deg)	46.48	(-10.23, 6.57)	43.33	(-8.96, 11.51)
Strike (deg)	51.31	(-12.08, 2.13)	43.09	(-5.32, 13.28)
<i>Okada</i>				
X (km)	0.23	(-0.74, 0.13)	0.10	(-0.51, 0.2)
Y (km)	0.12	(-0.43, 0.17)	0.08	(-0.36, 0.3)
Depth (km)	4.83	(-0.18, 0.31)	5.1	(-0.64, 0.1)
Opening (m)	1.98	(-0.03, 0.03)	1.99	(-0.04, 0.02)
Length (m)	3.02	(-0.23, 0.09)	2.96	(-0.26, 0.15)
Width (m)	2.01	(-0.3, 0)	2.01	(-0.4, 0.09)
Dip (deg)	50.01	(-8.69, 1.53)	43.11	(-3.64, 9.01)
Strike (deg)	139.38	(-18.94, 0)	132.65	(-6.63, 7.25)

<sup>a</sup>Estimated parameters of three source types (Mogi, Yang, and Okada). The confidence regions are calculated at the 95% confidence level.

are initiated with a starting temperature of 1, temperature reduction of 0.5, a maximum iteration and maximum success in each temperature of 500 and 200, respectively, and a final temperature of  $10^{-10}$ . The RISC-GA parameters are initiated with an initial population size of 40, a mutation rate of 0.5, a selection rate of 50%, and number of iterations of 100. The results of the RISC-SA and GA are shown in Table 3 and Figure 5. The two inversion algorithms produce the original observation almost perfectly, and residuals are in a range of about  $\pm 6$  mm. We observe a slight difference between the estimated confidence intervals, which are systematically narrower for the RISC-SA than for the RISC-GA. This means that either the precision of the RISC-SA result is higher than RISC-GA or the freedom of RISC-SA to explore the vicinity of the global solution is lower than RISC-GA. But when considering the amount of observation noise, both of them are reliable and hence acceptable. To compare the computation duration, we tested all calculations in this paper using MATLAB 7.1 software in a standard Windows XP platform with a 3.4 GHz processor. The computation times are summarized in Table 4 and show that RISC-GA is efficient and able to treat large or even full data sets.

[31] For the ellipsoidal Yang source, we have implemented exactly the same parameters as before. The inversion results are shown in Table 3 and Figure 5b. Although we added a high amount of noise, the results are considered to be quite good and are close to the initial model value (Table 3). Additionally, the inversion residuals are within the range of the observation noise. Although we are considering a broad deformation area (the sides are 10 times the Yang semimajor axis), the confidence length of the plunge and strike angle is considerably larger than the others, which shows the high uncertainty in estimating these parameters.

[32] In the third synthetic test, we inverted the surface deformation field caused by a rectangular dislocation source. The results are shown in Table 3 and Figure 5c. Although the inversion model reproduces the actual observation well and the inversion residuals are in the range of the observation noise, the uncertainty of the strike angle and width is clearly larger than the others.

[33] To summarize after these three tests, (1) both RISC algorithms were able to retrieve the initial model almost perfectly, even with the addition of high noise, (2) the presented algorithm for simultaneous confidence interval estimation works properly in both algorithms, and (3) for equal conditions, RISC-GA appears to be more efficient in terms of computation time. In the following, we use a real database from one of the most actively deforming volcanic system.

## 5. Application to Real InSAR Data From the Campi Flegrei Caldera Volcano

[34] Campi Flegrei (CF) is a caldera with a long documented history of unrest. It is also in one of the most densely populated regions in Italy, including part of the city of Naples, with about one million inhabitants. The historical period of deformation at CF culminated in 1158 and in 1538 A.D. [Bodnar et al., 2007]. The dominant type of historical

**Table 4.** Comparison of the Computation Time for the Synthetic Test Using RISC-SA and RISC-GA

Source Type	RISC-SA CPU Time (s)	RISC-GA CPU Time (s)
Mogi	832	38
Yang	1520	393
Okada	3982	832

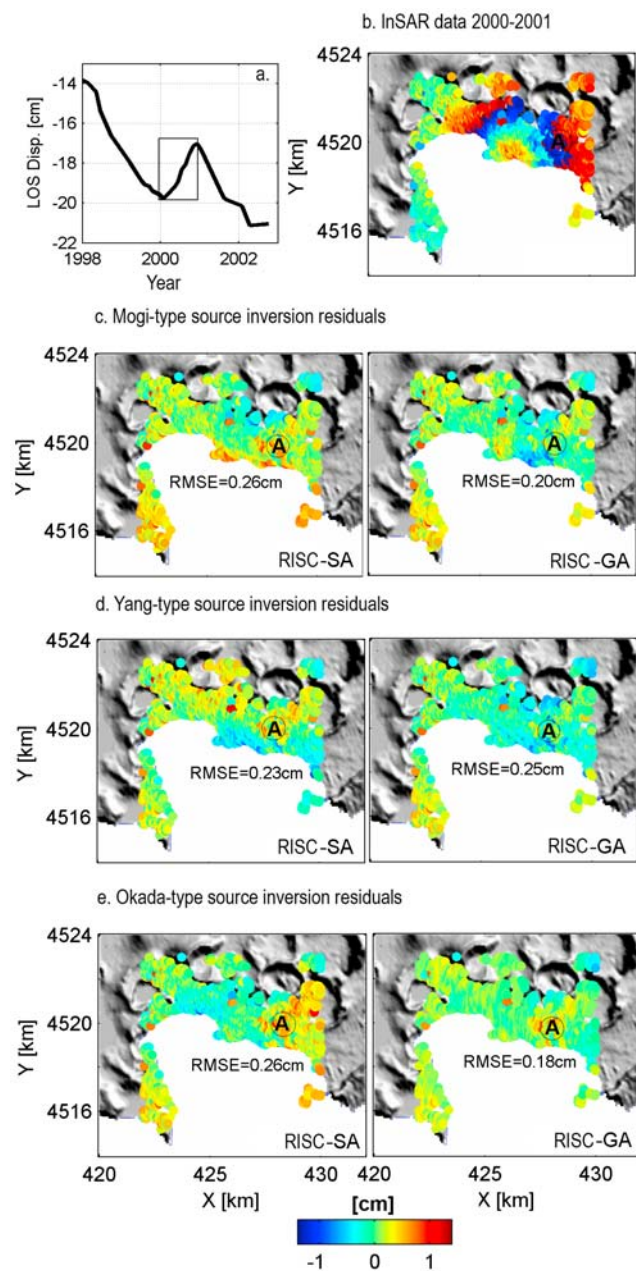


**Figure 6.** Application of the algorithm to real data from Campi Flegrei caldera, Italy. (a) A period of uplift occurred from 2000 to 2001 and is tested herein, (b) uplift observation in the LOS direction of ERS radar images in descending mode wrapped into 2.8 cm fringes, (c) residuals for Mogi-type source inversion by RISC-SA and RISC-GA, (d) residuals for Yang-type source inversion, and (e) residuals for Okada-type source inversion. All source types provide very good solutions with residuals below 1 cm. (A is the location of local hydrothermal activity in Solfatara.)

deformation in CF is subsidence, at a rate of 1.5–1.7 cm/a with occasional periods of uplift [Troise *et al.*, 2007]. The last major periods of uplift occurred in 1969–1972 and 1982–1984 [Barberi *et al.*, 1984] and have been observed by triangulation and trilateration networks [Troise *et al.*, 2007]. After the development of space geodetic techniques, especially InSAR, the monitoring value of measuring

deformations broadly increased. Subsidence at CF was already detected using the InSAR method by Avallone *et al.* [1999], who observed subsidence of up to 2.5 cm/a during the period 1993–1996. By using a gradient-based inversion method for an inflating Mogi-type point source, the same authors estimated the depth of the deformation source to be around 2.7 km. Lundgren *et al.* [2001] studied a longer InSAR time series and found continuing subsidence in the period 1993–1998. The estimated mean subsidence rate in this period is about 3.5 cm/a [Lundgren *et al.*, 2001]. To assess the source of the deformation, Lundgren and colleagues implemented a Levenberg-Marquardt nonlinear global optimization algorithm and investigated parameters of three different volcanic deformation sources (Mogi, Yang, Okada). They found source depths of about 2.5–3.0 km. Subsidence continued until 2000 and then changed to uplift, as shown by Lanari *et al.* [2004]. To model the source of deformation, they adapted a nonlinear least squares inversion for ellipsoidal (Yang) and rectangular (Okada) source parameters in an elastic homogeneous half-space and estimated a magma chamber depth of about 2.7–3.0 km. In other studies, such as those by Troise *et al.* [2007], Battaglia *et al.* [2006], and Gottsmann *et al.* [2006], different kinds of geophysical observations and inversion methods, such as gradient-based approaches for source parameters in an elastic homogeneous half-space, have been applied and estimated the deformation source similarly to be at a depth of about 2.5–3.0 km. In a recent study, Amoroso *et al.* [2007] discussed another uplift period lasting from 2004 to 2006 and modeled this phenomenon in a horizontally layered half-space. They obtained an estimate of 3.5 km depth for a crack-type deformation source.

[35] However, seismic studies suggest a more complex story about the 3-D location of the hydrothermal and magma chamber. On the basis of the seismic tomography, two low-velocity zones can be inferred at depths of 2.7 and 7.5 km [Zollo *et al.*, 2008]. The shallower zone might be interpreted as a thermometamorphic rock assembly, while the deeper one may be interpreted as a magma body with an area of less than 30 km<sup>2</sup> and a thickness of 1.2–1.5 km [Zollo *et al.*, 2008].

[36] In the following, we test the two improved RISC methods on the episodes of uplift (2000–2001) and subsidence (2001–2002). Utilizing both genetic algorithm and simulated annealing, we estimate the deformation source parameters as well as their uncertainty.

### 5.1. Data Set

[37] The data set used here is extracted from the geodetic time series obtained by a small base line subset (SBAS) approach for measuring ground displacement using differential SAR interferometry [Lanari *et al.*, 2004]. This SBAS technique selects data pairs with a small baseline to establish differential interferograms for achieving time series analysis. The advantages of this method are in overcoming spatial decorrelation and in eliminating atmospheric artifacts, as detailed by Bernardino *et al.* [2002].

[38] The time series of a long period of subsidence from 1992 until 2002, with a cumulative displacement of 25 cm in the center of the caldera, has been presented by Bernardino *et al.* [2002]. The subsidence episode reversed into uplift in 2000. The uplift episode lasted 1 year, accumulating about

**Table 5.** Inversion Results of the Uplift at Campi Flegrei Observed by InSAR Over the Period 2000–2001<sup>a</sup>

Parameter	Simulated Algorithm		Genetic Annealing	
	Inversion Result	Confidence Interval (95%)	Inversion Result	Confidence Interval (95%)
<i>Mogi</i>				
X (km)	426.20	(−0.1, 0.08)	426.22	(−0.36, 0.24)
Y (km)	4519.45	(−0.41, 0.31)	4519.65	(−1.34, 0)
Depth (km)	2.41	(−0.3, 0.31)	2.29	(0, 0.92)
Volume change (km <sup>3</sup> )	0.00091	(−0.0002, 0.0003)	0.00073	(0, 0.0007)
<i>Yang</i>				
X (km)	426.05	(−0.3, 0.29)	426.54	(−1.42, 0)
Y (km)	4519.80	(−0.58, 0.37)	4519.66	(−0.74, 0.57)
Depth (km)	2.84	(0, 0.5)	2.89	(−0.36, 0.4)
Pressure change (GPa)	0.00074	(0, 0.0009)	0.00069	(0, 0.0047)
Major Axis (km)	2.68	(−0.75, 0.08)	2.77	(−0.52, 0.02)
Minor Axis (km)	1.43	(−0.18, 0.01)	1.46	(−0.81, 0)
Plunge (deg)	82.40	(−14.47, 0)	87.98	(−19.13, 0)
Strike (deg)	91.71	(−0.14, 21.49)	113.39	(−22.12, 0)
<i>Okada</i>				
X (km)	426.16	(−0.96, 0)	425.86	(−0.31, 0.63)
Y (km)	4518.17	(−0.9, 1.17)	4518.47	(−0.85, 0.53)
Depth (km)	3.26	(−0.88, 0)	3.02	(−0.47, 0.09)
Opening (m)	1.08	(−0.45, 0)	0.84	(−0.12, 0.8)
Length (m)	0.44	(0, 0.52)	0.69	(0, 0.89)
Width (m)	1.45	(0, 0.22)	1.51	(−0.69, 0.04)
Dip (deg)	62.39	(−3.15, 20.87)	76.29	(−37.62, 0)
Strike (deg)	103.86	(−32.34, 0)	118.52	(−43.91, 0)

<sup>a</sup>Parameters of three source types (Mogi, Yang, and Okada) are estimated. The confidence regions are calculated at the 95% confidence level.

4 cm of displacement. Another subsidence episode followed in 2001 and continued to the end of the time span considered here. We now compare the source parameters of the 1 year uplift and 1 year subsidence periods and consider the observation error and model deficiency. We calculate a confidence interval for all parameters as well as their best estimates.

## 5.2. Model Uplift Period 2000–2001

[39] To initialize RISC-SA and RISC-GA, we follow the same procedure as detailed in the synthetic simulations in section 4 and define upper and lower bounds in search space. For both deformation periods (uplift and subsidence) and for all types of model sources, the considered bounds of depth range is assumed to be somewhere between 2 and 5 km, as suggested in previous publications [e.g., *De Natale et al.*, 1997; *Battaglia et al.*, 2006]. Equation (10) allows us to estimate the lower bound of the volume change, which is  $5 \times 10^{-4}$  km<sup>3</sup>. The Mogi-type source volume change lies between  $5 \times 10^{-4}$  and  $5 \times 10^{-2}$  km<sup>3</sup>, and the horizontal location could be at any point in the observation plane. Tables 5 and 6 summarize the results and computation times for RISC-SA and RISC-GA, and a graphical representation is given in Figure 6. The root-mean-square error (RMSE) for both methods is about 0.3 cm (i.e., similar to observation error) and shows that the model reproduces the observations very well. The depth and volume change differ slightly in RISC-SA and RISC-GA. However, considering their confidence intervals, we note that both inversions are consistent, covering a similar range of uncertainty.

[40] The second model was a Yang-type source. As in the previous case, we start with a broad bound for the parameters, with an assumed pressure bound between 0 and 0.01 GPa, a semiaxis between 0 and 3 km, a dip angle between 0 and 90°, a strike angle between 30° and 150°,

and the horizontal location at any point in the observation plane. The RMSE for both RISC-SA and RISC-GA is again about 0.3 cm, which shows that the models precisely reproduced the observation field. The best fitting source is elongated east-west, and the estimated depth is in the range of 2.5–3.3 km.

[41] As a third model, we consider an Okada-type source. The model parameters are bound by a 0–2 km length and width, a 0–90° dip, a 30°–150° strike, and a 0–2 m opening. Again, this source model can reproduce the deformation field very well, with an RMSE below 0.3 cm. The Okada source is elongated east-west, and the associated depth varies between ~2.4 and ~3.3 km.

## 5.3. Model Subsidence Period 2001–2002

[42] To initiate RISC-SA and RISC-GA, we considered a bound between  $5 \times 10^{-4}$  to  $5 \times 10^{-2}$  km<sup>3</sup> for a Mogi-type volume change, and the whole observation plane for the horizontal location. The results are provided in Table 7 and Figure 7. The RMSE is about 0.5 cm; thus, the model reproduces well the InSAR observations. Because the numbers of observation points and optimization parameters are exactly the same as for the uplift case, the computation times remain similar. We use similar parameter bounds the subsidence scenario in the inversion method described above.

[43] The estimated depth for the source is between ~2.1 and ~2.4 km for RISC-SA and between ~2.2 and ~2.8 km

**Table 6.** Comparison of the Computation Time for Inverting the Uplift Period Deformation Data Set Using RISC-SA and RISC-GA

Source Type	RISC-SA CPU Time (s)	RISC-GA CPU Time (s)
Mogi	283	13
Yang	677	26
Okada	1354	51

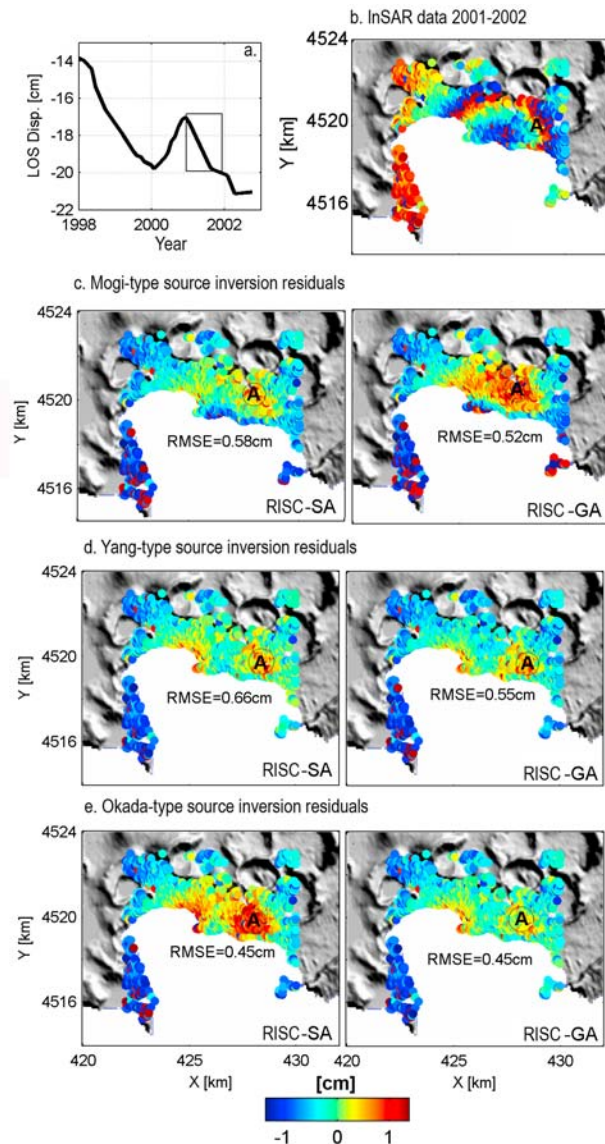


**Figure 7.** Application of algorithm to real data from Campi Flegrei caldera, Italy. (a) A period of subsidence from 2001 to 2002, (b) subsidence observation in the LOS direction of ERS radar images in descending mode (compare Figure 6), (c) residuals for Mogi-type source inversion by RISC-SA and RISC-GA, (d) residuals for Yang-type source inversion, and (e) residuals for Okada-type source inversion. All plots are wrapped into 2.8 cm fringes. All source types provide good solutions, with smallest residuals for the Okada type.

for RISC-GA, while the optimum solution is found at a 2.3 km depth for both.

[44] The RMSE for the Yang-type is larger than for the Mogi-type source, which may be due to the low sensitivity of the source parameters (section 2). The Yang source is elongated east-west and the depth range is  $\sim 2.4$  to  $\sim 2.9$  km for both RISC-SA and RISC-GA. Comparing this depth with the uplift, the inversion suggests that the source is shallower than for the inflation period.

[45] The Okada-type results show a better fit than those for the Yang-type source because of the higher sensitivity of

the Okada parameters. The estimated depth for RISC-SA is between  $\sim 2.2$  and  $\sim 3.0$  km and between  $\sim 2.3$  and  $\sim 3.1$  km for RISC-GA.

## 6. Discussion

[46] In a sensitivity test, we investigated the influence of an analytical model on the quality of the inversion results. We found that a poor analytical model may lead to unreliable results. Devising a gradient-free, fast and reliable optimization method, which is necessary for semi-real-time hazard assessment, we considered two sophisticated optimization approaches, simulated annealing (SA) and genetic algorithm (GA). We utilized their advantages and suggested a method to overcome their disadvantages, by including a hybrid randomly iterated search and statistical competency approach (RISC). To show the reliability and efficiency of the RISC approach, we performed synthetic and real case tests. In the following, we discuss different theoretical and practical aspects of the presented approach.

### 6.1. Sensitivity Analysis

[47] In sensitivity tests, we considered the mutual effects of parameters and observation errors (in the same geometry as the ERS satellite image in descending mode). We suggested that the reliability of the parameters is not only dependent on the observation quality but is also strongly affected by the observation distribution because of model sensitivity. As a result, we recommend in such inversion problems the use of an entire data set including near- and far-field observations with suitable relative weighting. For instance, weighting of the far field improves the quality of the plunge angle, whereas weighting the near field improves the quality of the pressure change in the case of a Yang-type source.

[48] It has been shown by *Dieterich and Decker* [1975] that the source geometry and depth using vertical deformation data alone cannot be reliably resolved and that the full 3-D displacement field is needed. Because InSAR observations are only a projection of the 3-D displacement field, some of the source parameters may not be resolved reliably. However, very often in the InSAR applications, we are able to carry out joint inversions by combining observations obtained from different satellite geometries. To see how these extra observations influenced the quality of the parameters, we set up two other sensitivity tests, the results of which are illustrated in the auxiliary material. The first test considered the ERS satellite image geometry in ascending mode, and the second test considered the norm of the 3-D displacement field obtained, for instance, by combining InSAR, GPS, and leveling data. We found a moderate improvement in the sensitivity of the model parameters in comparison with previous results. In the case of the Okada-type source, the width and strike angles remain nonunique, while the quality of the other parameters is clearly improved. Considering the sensitivity test for ascending and descending geometry, together with the norm of the 3-D displacement field, we suggest that the analytical model sensitivity (termed condition number after equation (5)) might be a significant foundation for occasional poor observations and parameter interactions. Therefore, even though we were able to set up joint inversion of

**Table 7.** Inversion Results of the Subsidence at Campi Flegrei Observed by InSAR Over the Period 2001–2002<sup>a</sup>

Parameter	Simulated Algorithm		Genetic Annealing	
	Inversion Result	Confidence Interval (95%)	Inversion Result	Confidence Interval (95%)
<i>Mogi</i>				
X (km)	426.54	(−0.05, 0.05)	426.57	(−0.46, 0)
Y (km)	4519.34	(−0.23, 0.27)	4519.80	(−0.76, 0.15)
Depth (km)	2.31	(−0.2, 0.12)	2.32	(−0.12, 0.53)
Volume change (km <sup>3</sup> )	−0.00106	(−0.0002, 0.0002)	−0.00097	(−0.0006, 0)
<i>Yang</i>				
X (km)	426.03	(−0.35, 0)	426.31	(−0.25, 0.47)
Y (km)	4518.51	(0, 0.14)	4519.53	(−0.75, 0)
Depth (km)	2.41	(0, 0.15)	2.38	(0, 0.52)
Pressure change (GPa)	−0.00224	(−0.0036, 0)	−0.00305	(−0.0023, 0)
Major axis (km)	2.43	(0, 0.45)	2.09	(0, 0.38)
Minor axis (km)	1.00	(−0.39, 0)	0.73	(−0.08, 0.23)
Plunge (deg)	63.50	(0, 11.61)	88.38	(−23.24, 0)
Strike (deg)	117.73	(−23.05, 0)	111.88	(−17.19, 0)
<i>Okada</i>				
X (km)	426.42	(−0.19, 0.2)	426.44	(−0.49, 0.16)
Y (km)	4519.04	(−0.56, 0.33)	4518.97	(−0.88, 0)
Depth (km)	2.66	(−0.43, 0.31)	2.88	(−0.56, 0.22)
Opening (m)	−1.51	(−0.36, 0.49)	−1.49	(−0.14, 0.4)
Length (m)	0.98	(−0.41, 0.27)	0.86	(−0.07, 0.35)
Width (m)	0.53	(0, 0.3)	0.70	(0, 0.31)
Dip (deg)	73.97	(−21.47, 2.62)	73.97	(−21.47, 2.62)
Strike (deg)	118.04	(−19.47, 0)	115.27	(−18.25, 0)

<sup>a</sup>Parameters of three source types (Mogi, Yang, and Okada) are obtained. The confidence regions are calculated at the 95% confidence level.

different geometries, good coverage of deformation in the near and far field and/or independent geophysical data (seismicity, gravity) still seems necessary.

## 6.2. Advances of the RISC Approach

[49] We proposed the RISC approach as a novel technique for answering the demand of practical optimization problems in obtaining a reliable and fast solution. Nevertheless, a valid question remains as to whether other optimization methods (listed in Table 1) are not able to find the optimal solution equally well. From mathematical point of view it has been proved that all those optimization techniques are able to reach a global solution, though at expense of CPU time (because in many scenarios the computation time approaches infinity, and defining a unique search criteria that is large enough is difficult). In practical optimization problems the CPU time is limited, the search criteria are problem-dependent, and priori information is poorly available. Therefore, any of those standard techniques may fail in finding the global solution; a failure that is not defined as inherent but is rather the result of our poor knowledge about search space and CPU time constraint. Therefore, in practical cases it seems reasonable to be aware of this shortcoming. The RISC approach presented here is an attempt to answer the request of practical problems for reliable and efficient estimation of the global solution. In the RISC approach, the optimization problem can be initialized with reasonable values based on available information and user experiences; the algorithm converges to a good approximation of the global solution. In fact the RISC approach is not a stand-alone optimization technique, rather it further strengthens available search techniques, with the aim of improving reliability and efficiency of the optimization process. In this study we exemplified this with a combination of GA and SA, but this approach may be adapted as well for any other algorithms such as covariance matrix adoption

evolutionary strategy [Igel *et al.*, 2007] or neighborhood approach [Sambridge, 1999b].

[50] The main limitation of the existing algorithms is their tendency to become trapped in a local minimum because, for example, of an inappropriate cooling schedule. An improvement is shown by combining the standard SA with a randomly iterative (RI) approach. The same approach could be applied to the simple GA, especially when dealing with a complex search space. Another important aspect is obtaining a confidence region for the parameters by implementing a statistical competency (SC) approach. The statistic used here considers observation quality and model

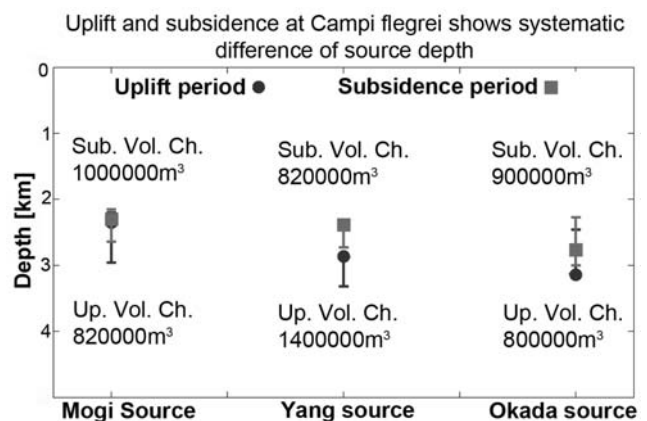


**Figure 8.** Synthesis of the Campi Flegrei test. Comparison of the absolute depth, associated confidence interval and volume change of different deformation source types (Mogi, Yang, and Okada) for the two periods of uplift (2000–2001) and subsidence (2001–2002). The uplift period is systematically associated with a deeper source than the subsidence period.

**Table 8.** Comparison Between the Depths of Different Deformation Sources Obtained in This Study Using RISC-SA and RISC-GA Approaches and Earlier Studies

Source Type	Reference	Depth (km)	Inversion Method
Mogi	This study	2.1–3.2	RISC-GA/SA
	Lundgren <i>et al.</i> [2001]	2.5	Levenberg-Marquardt
Yang Spherical source	This study	2.1–3.2	RISC-GA/SA
	Avallone <i>et al.</i> [1999]	2.7	Gradient search
	Lundgren <i>et al.</i> [2001]	2.1	Levenberg-Marquardt
	Lanari <i>et al.</i> [2004]	2.4–3.2	Least squares
	Battaglia <i>et al.</i> [2006]	1.9–2.2	Least squares
Okada	This study	2.4–3.3	RISC-GA/SA
	Lundgren <i>et al.</i> [2001]	2.9	Levenberg-Marquardt
Penny-shaped crack	Lanari <i>et al.</i> [2004]	2.4–2.8	Least squares
	Battaglia <i>et al.</i> [2006]	2.5–3.5	Least squares

deficiency together. Combining RI and SC, we presented a sophisticated inversion algorithm. This approach can be applied to any other heuristic search algorithm to improve the performance of the search operator. The MATLAB codes for both RISC-SA and RISC-GA are included in the auxiliary material.

### 6.3. Model Implications for Campi Flegrei Volcano

[51] The presented InSAR time series showed a general trend of subsidence from 1992 to 2002, temporarily interrupted by the 2000 uplift period. The uplift reached up to 4 cm between 2000 and 2001 and was followed by subsidence of up to 5 cm in 2002. The model that best fits both episodes is obtained by an Okada-type source, although also the other models also reproduced the observed deformation field well. We found that during the subsidence period, the source of deformation is systematically shallower and the volume change is larger than during the uplift episode (see Figure 8). The source separation is on average about 0.6 km. Because our sensitivity test showed a 50% change in the average depth compromising by almost 200% change in the surface observation, we are confident that this separation ( $\sim 0.6$  km equivalent to 25% change in the observed deformation field) is not because of poor observation precision or the applied inversion method. Moreover, this result is similar to what Battaglia *et al.* [2006] obtained on the basis of inverting geodetic and gravity data for the uplift period of 1980–1984 and the subsidence period of 1990–1995. The source depth in our model, however, is slightly deeper. Table 6 compares the RISC result and other published studies, showing that the independent studies are agreeing well. On the basis of previous sensitivity tests, we note that the location and strength parameters are well constrained, whereas the strike and dip parameters could not be uniquely determined.

[52] Considering model deficiency and observation variance via a statistical approach, we calculated the confidence region for the parameters. For instance, the uncertainty of the source depth is between 2.1 and 3.3 km for the uplift and between 2.1 and 3.0 km for the subsidence period. This range covers most of the estimates using the elastic homogeneous assumption in the Campi Flegrei region (Table 8).

[53] Nevertheless, our estimate is not completely consistent with the seismically inferred reservoir, where two zones can be inferred at depths of 2.7 and 7.5 km [Zollo *et al.*, 2008]. This discrepancy might be due to material heteroge-

neity and observation uncertainty or because of an oversimplified base model. The effect of reactivated steeply dipping ring faults may explain such a discrepancy [De Natale *et al.*, 1997]. Another source of the difference may be found in the simplified half-space assumption. Amoroso *et al.* [2007] studied the unrest period of 1982–1984 at the CF caldera using a crack model embedded in the layered elastic half-space. The obtained PDF for the depth of the best model as a quality criterion is between 2 and 5 km. This broad estimate includes the estimated confidence region in this paper. Therefore, the slight differences between various models might be due to differences either in observation quality or model assumptions. Although our base model is very simple, our inversion approach is applicable to more complex or simpler scenarios and significantly improves data resolution and computation time, and thus the efficiency and robustness of geodetic data interpretations.

## 7. Conclusions

[54] We applied a simulated annealing and genetic algorithm for estimating deformation source parameters based on surface displacement data. The work was aimed at developing a fast and reliable inversion technique that allows the utilization of large data sets with confidence. Therefore, we first showed that the important parameters for the precision and accuracy of the results are not only the quality of the observations but also the distribution of the observations. We further improved the optimization methods, by applying a hybrid random iterated search and statistical competency approach (RISC). The RISC approach prevents SA from getting trapped in local minima. Moreover, this approach allows an estimation of the quality of the results at a certain confidence level. We extended a similar idea to the GA for estimating the confidence interval of parameters. Similarly RISC can be applied to different optimization methods. To indicate the efficiency and robustness of our methods, we performed synthetic tests utilizing three commonly used volcano deformation sources, including the Mogi, Yang, and Okada sources. We found that the two algorithms can retrieve noisy synthetic field parameters as well as provide a meaningful confidence region for the results. Therefore, the statistical approach combined with an inversion algorithm has been shown to be a large improvement to the standard techniques commonly used. Considering

computational time, we found that GA is much faster than SA and also more flexible in accepting limits for parameters, which is useful in hybrid and constrained optimization and it allows consideration of full InSAR sets.

[55] We applied the two developed optimization methods to investigate the source of the deformation periods at Campi Flegrei volcano, Italy. The observations are a time series obtained on the basis of SBAS interferometry. The displacement series shows that an uplift period occurred in 2000–2001 and a subsidence period occurred in 2001–2002. As a result, for the uplift and subsidence periods the depth of the deformation source is constrained between 2.1 and 3.3 km and 2.1 and 3.0 km, respectively. A comparison of the source parameters for the uplift and subsidence periods showed that the source location is systematically deeper for the uplift period. We utilize an approach to validate the model parameters considering two different sources of uncertainty, model deficiency and observation errors.

[56] **Acknowledgments.** This work was financially supported by the R&D program GEOTECHNOLOGIEN funded by the German Ministry of Education and Research (BMBF) grant 03G0646B, the German Research Foundation (DFG) grant WA1642-1/4, and the Helmholtz Centre Potsdam, GFZ, German Research Centre for Geosciences. The SBAS-InSAR data utilized in the algorithm test and examples were kindly provided by R. Lanari. Detailed and constructive reviews and editorial remarks are greatly appreciated.

## References

- Amelung, F., S. H. Yun, T. R. Walter, P. Segall, and S. W. Kim (2007), Stress control of deep rift intrusion at Mauna Loa volcano, Hawaii, *Science*, *316*, 1026–1030, doi:10.1126/science.1140035.
- Amoruso, A., L. Crescentini, A. T. Linde, I. S. Sacks, R. Scarpa, and P. Romano (2007), horizontal crack in a layered structure satisfies deformation for the 2004–2006 uplift of Campi Flegrei, *Geophys. Res. Lett.*, *34*, L22313, doi:10.1029/2007GL031644.
- Avallone, A., P. Briole, C. Delacourt, A. Zollo, and F. Beauducel (1999), Subsidence at Campi Flegrei (Italy) detected by SAR interferometry, *Geophys. Res. Lett.*, *26*, 2303–2306, doi:10.1029/1999GL900497.
- Barberi, F., D. P. Hill, F. Innocenti, G. Luongo, and M. Treuil (Eds.) (1984), The 1982–1984 Bradyseismic crisis at Phlegrean Fields (Italy), *Bull. Volcanol.*, *47*, 173–411, doi:10.1007/BF01961546.
- Basu, A., and L. N. Frazer (1990), Rapid determination of critical temperature in simulated annealing inversion, *Science*, *249*, 1409–1412, doi:10.1126/science.249.4975.1409.
- Battaglia, M., P. Segall, J. Murray, P. Cervelli, and J. Langbein (2003), The mechanics of unrest at Long Valley caldera, California: 1. Modeling the geometry of the source using GPS, leveling and 2-color EDM data, *J. Volcanol. Geotherm. Res.*, *127*, 195–217, doi:10.1016/S0377-0273(03)00170-7.
- Battaglia, M., C. Troise, F. Obrizzo, F. Pingue, and G. De Natale (2006), Evidence for fluid migration as the source of deformation at Campi Flegrei caldera (Italy), *Geophys. Res. Lett.*, *33*, L01307, doi:10.1029/2005GL024904.
- Berardino, P., G. Fornaro, R. Lanari, and E. Sansosti (2002), A new algorithm for surface deformation monitoring based on small baseline differential SAR interferograms, *IEEE Trans. Geosci. Remote Sens.*, *40*, 2375–2383, doi:10.1109/TGRS.2002.803792.
- Bjerrhammar, A. (1973), *Theory of Errors and Generalized Matrix Inverse*, Elsevier, New York.
- Bodnar, R. J., C. Cannatelli, B. De Vivo, A. Lima, H. E. Belkin, and A. Milia (2007), Quantitative model for magma degassing and ground deformation (bradyseism) at Campi Flegrei, Italy: Implications for future eruptions, *Geology*, *35*, 791–794, doi:10.1130/G23653A.1.
- Carbone, D., G. Currenti, and C. Del Negro (2008), Multiobjective genetic algorithm inversion of ground deformation and gravity changes spanning the 1981 eruption of Etna volcano, *J. Geophys. Res.*, *113*, B07406, doi:10.1029/2006JB004917.
- Cervelli, P., M. Murray, P. Segall, Y. Aoki, and T. Kato (2001a), Estimating source parameters from deformation data, with an application to the March 1997 earthquake swarm off the Izu Peninsula, *J. Geophys. Res.*, *106*, 11,217–11,237, doi:10.1029/2000JB900399.
- Cervelli, P., M. H. Murray, P. Segall, Y. Aoki, and T. Kato (2001b), Estimating source parameters from deformation data, with an application to the March 1997 earthquake swarm off the Izu Peninsula, Japan, *J. Geophys. Res.*, *106*, 11,217–11,238, doi:10.1029/2000JB900399.
- Chevrot, S. (2002), Optimal measurement of relative and absolute delay times by simulated annealing, *Geophys. J. Int.*, *151*, 164–171, doi:10.1046/j.1365-246X.2002.01755.x.
- Currenti, G., C. Del Negro, and G. Nunnari (2005), Inverse modelling of volcanomagnetic fields using a genetic algorithm technique, *Geophys. J. Int.*, *163*, 403–418, doi:10.1111/j.1365-246X.2005.02730.x.
- Davis, L. (1987), *Genetic Algorithms and Simulated Annealing*, Pitman, London.
- Davis, P. M. (1986), Surface deformation due to inflation of an arbitrarily oriented triaxial ellipsoidal cavity in an elastic half-space, with reference to Kilauea volcano, Hawaii, *J. Geophys. Res.*, *91*, 7429–7438, doi:10.1029/JB091iB07p07429.
- Dawson, J., and P. Tregoning (2007), Uncertainty analysis of earthquake source parameters determined from InSAR: A simulation study, *J. Geophys. Res.*, *112*, B09406, doi:10.1029/2007JB005209.
- Deb, K., S. Agrawal, A. Pratap, and T. Meyarivan (2000), A fast elitist non-dominated sorting genetic algorithm for multi-objective optimisation: NSGA-II in *Proceedings of the 6th International Conference on Parallel Problem Solving from Nature*, Lecture Notes In Computer Science; Vol. 1917, pp. 849–858, Springer, New York.
- De Natale, G., S. M. Petrazzuoli, and F. Pingue (1997), The effect of collapse structures on ground deformations in calderas, *Geophys. Res. Lett.*, *24*, 1555–1558, doi:10.1029/97GL01600.
- Dieterich, J. H., and R. W. Decker (1975), Finite element modeling of surface deformation associated with volcanism, *J. Geophys. Res.*, *80*, 4094–4102, doi:10.1029/JB080i029p04094.
- Dzurisin, D. (2006), *Volcano Deformation: Geodetic Monitoring Techniques*, Springer, Berlin.
- Goldberg, D. E. (1989), *Genetic Algorithms in Search, Optimization, and Machine Learning*, Addison-Wesley, Reading, Mass.
- Gottsmann, J., A. G. Camacho, K. F. Tiampo, and J. Fern'andez (2006), Spatiotemporal variations in vertical gravity gradients at the Campi-Flegrei caldera (Italy): A case for source multiplicity during unrest?, *Geophys. J. Int.*, *167*, 1089–1096, doi:10.1111/j.1365-246X.2006.03157.x.
- Haupt, R. L., and S. E. Haupt (2004), *Practical Genetic Algorithms*, John Wiley, Hoboken, N. J.
- Holland, J. H. (1975), *Adaptation in Natural and Artificial Systems*, Univ. of Mich. Press, Ann Arbor, Mich.
- Holland, J. H. (1992), Genetic algorithms, *Sci. Am.*, *267*, 66–72.
- Igel, C., N. Hansen, and S. Roth (2007), covariance matrix adaptation for multi-objective optimization, *Evol. Comput.*, *15*, 1–28, doi:10.1162/evco.2007.15.1.1.
- Jónsson, S., H. Zebker, P. Segall, and F. Amelung (2002), Fault slip distribution of the Mw 7.1 Hector Mine, California, earthquake, estimated from satellite radar and GPS measurements, *Bull. Seismol. Soc. Am.*, *92*, 1377–1389, doi:10.1785/0120000922.
- Keilis-Borok, V. I., and T. B. Yanovskaja (1967), Inverse problems of seismology, *Geophys. J. R. Astron. Soc.*, *13*, 223–234.
- Kirkpatrick, S. C., D. Gelatt, and M. P. Vecchi (1983), Optimization by simulated annealing, *Science*, *220*, 671–680, doi:10.1126/science.220.4598.671.
- Lanari, R., P. Berardino, S. Borgström, C. Del Gaudio, P. De Martino, G. Fornaro, S. Guarino, G. P. Ricciardi, E. Sansosti, and P. Lundgren (2004), The use of IFSAR and classical geodetic technique for caldera unrest episode: Application to Campi Flegrei uplift event of 2000, *J. Volcanol. Geotherm. Res.*, *133*, 247–260, doi:10.1016/S0377-0273(03)00401-3.
- Lundgren, P., S. Usai, E. Sansosti, R. Lanari, M. Tesauro, G. Fornaro, and P. Berardino (2001), Modeling surface deformation observed with synthetic aperture radar interferometry at Campi Flegrei caldera, *J. Geophys. Res.*, *106*, 19,355–19,366, doi:10.1029/2001JB000194.
- McTigue, D. F., and P. Segall (1988), Displacements and tilts from dip-slip faults and magma chambers beneath irregular surface topography, *Geophys. Res. Lett.*, *15*, 601–604, doi:10.1029/GL015i006p00601.
- Metropolis, N., M. N. Rosenbluth, A. W. Rosenbluth, A. H. Teller, and E. Teller (1953), Equation of state calculations by fast computing machines, *J. Chem. Phys.*, *21*, 1087–1092, doi:10.1063/1.1699114.
- Michalewicz, Z. (1994), *Genetic Algorithms + Data Structures = Evolution Programs*, 2 ed., Springer, New York.
- Mogi, K. (1958), Relations between the eruptions of various volcanoes and the deformations of the ground surfaces around them, *Bull. Earthquake Res. Inst. Univ. Tokyo*, *36*, 99–134.
- Okada, Y. (1985), Surface deformation due to shear and tensile faults in a half-space, *Bull. Seismol. Soc. Am.*, *75*, 1135–1154.

- Rawlins, G. J. E. (1991), *Foundations of Genetics Algorithms*, Morgan Kaufmann, San Mateo, Calif.
- Rothman, D. H. (1985), Nonlinear inversion statistical mechanics, and residual statics corrections, *Geophysics*, *50*, 2784–2796, doi:10.1190/1.1441899.
- Sambridge, M. (1998), Exploring multi-dimensional landscapes without a map, *Inverse Probl.*, *14*, 427–440, doi:10.1088/0266-5611/14/3/005.
- Sambridge, M. (1999a), Geophysical inversion with a neighbourhood algorithm, I, Searching a parameter space, *Geophys. J. Int.*, *138*, 479–494, doi:10.1046/j.1365-246X.1999.00876.x.
- Sambridge, M. (1999b), Geophysical inversion with a neighbourhood algorithm, II, Appraising the ensemble, *Geophys. J. Int.*, *138*, 727–746, doi:10.1046/j.1365-246x.1999.00900.x.
- Sambridge, M., and K. Mosegaard (2002), Monte Carlo methods in geophysical inverse problems, *Rev. Geophys.*, *40*(3), 1009, doi:10.1029/2000RG000089.
- Troise, C., G. De Natale, F. Pingue, F. Obrizzo, P. De Martino, U. Tammaro, and E. Boschi (2007), Renewed ground uplift at Campi Flegrei caldera (Italy): New insight on magmatic processes and forecast, *Geophys. Res. Lett.*, *34*, L03301, doi:10.1029/2006GL028545.
- Vanicek, P., and E. Krakiwesky (1982), *Geodesy: The Concepts*, North-Holland, Amsterdam.
- Whitley, D. L. (1994), A genetic algorithm tutorial, *Stat. Comput.*, *4*, 65–85, doi:10.1007/BF00175354.
- Yang, X.-M., P. M. Davis, and J. H. Dieterich (1988), Deformation from inflation of a dipping finite prolate spheroid in an elastic half-space as a model for volcanic stressing, *J. Geophys. Res.*, *93*, 4249–4257, doi:10.1029/JB093iB05p04249.
- Zhou, R., F. Tajima, and P. L. Stoffa (1995), Application of genetic algorithm to constrain near-source velocity structure for 1989 Sichuan earthquake, *Bull. Seismol. Soc. Am.*, *85*, 590–605.
- Zollo, A., N. Maercklin, M. Vassallo, D. Dello Iacono, J. Virieux, and P. Gasparini (2008), Seismic reflections reveal a massive melt layer feeding Campi Flegrei caldera, *Geophys. Res. Lett.*, *35*, L12306, doi:10.1029/2008GL034242.

---

M. Shirzaei and T. R. Walter, Section 2.1, Department of Physics of the Earth, Deutsches GeoForschungsZentrum, Telegrafenberg, D-14473 Potsdam, Germany. (shirzaei@gfz-potsdam.de)